RSC Advances

PAPER

A facile chemical method for the synthesis of 3C–SiC nanoflakes

Mirela Dragomir,*[ab] Matjaz Valant,[ac] Mattia Fanetti[a] and Yurij Mozharivskyj[b]

A facile chemical method for the synthesis of 3C–SiC nanoflakes is presented. The process involves the pyrolysis of polycarbosilane (PCS) at 700 °C, in a NaCl powder template, followed by thermal treatment at 1200 °C. The salt is easily removed by washing with water. The morphology of the SiC particles is found to be dependent on the NaCl/PCS weight ratio and by carefully tuning this ratio, different SiC structures can be obtained. While at NaCl/PCS ratios < 40 : 1 micrometer-sized particles with a foamy like structure result, a NaCl/PCS ratio of 40 : 1 is crucial for the formation of 3C–SiC nanoflakes. These nanoflakes are less than 5 nanometers thick, have a high specific surface area of 169 m^2 g^{-1} and a high total pore volume of up to 0.75 cm^3 g^{-1}. This method could open a simple, versatile and robust way for the production of SiC nanostructures. Such a facile synthetic method could bring nanostructured SiC one step closer to the ultimate goal of practical applications.

Introduction

The technological potential of nanostructured 3C–SiC is enormous due to its exceptional properties such as high mechanical strength over weight ratio, chemical and thermal stability, biocompatibility,[1–3] and low band gap[4] of 2.4 eV combined with a high value for electron mobility.[5]

Many novel properties and applications have been reported and predicted for nanosized 3C–SiC, such as nanoscale light emitters,[6–9] photocatalysis,[10–12] Li-ion batteries,[13] hydrogen evolution and storage,[14–17] support for graphene growth,[18] for strengthened structural polymer nanocomposites,[19,20] and others.[21,22] In addition, a number of current technologies are standing by for a chance to introduce SiC nanopowder in their products immediately when it will be commercially viable. An example is the car tire industry where the SiC nanopowder as an additive to rubber could dramatically reduce wear and increase lifetime of the product.

It is surprising that despite the obvious technological potential and commercial interest, the synthesis of SiC nanostructures remains technologically complex and energy consuming. No facile methods for mass production of the SiC nanopowder have yet been developed. The limitations of the existing synthetic methods hinder the development of products and devices based on the nanostructured SiC.

Compared to oxide nanoparticles that require only mild synthetic conditions and simple procedures, far fewer synthetic

methods exist for the synthesis of non-oxide compounds such as 3C–SiC, despite all efforts and recent progress. The available synthetic approaches for nanosized 3C–SiC such as pulsed laser ablation,[23] arc discharge,[24] chemical vapour deposition,[25] carbothermal reduction,[26–30] or laser pyrolysis[31] suffer major disadvantages as they are technically demanding and require very high temperatures ($\gg$1500 °C), long reaction times or sophisticated and expensive equipment. Hence, during the last years, researchers' attention has been devoted to alternative synthetic routes that would enable economically viable mass production of SiC nanopowders. Alternative methods such as molten salt route,[32] chemical etching in aqueous HF[33] or pyrolysis of organosilicon polymers in nanotemplates have been reported.[34,35] However, these methods have their drawbacks; they use expensive irrecoverable templates (e.g., nanosized silica)[36] or concentrated HF as an etching agent. Consequently, these approaches make the production of nanosized SiC unsustainable.

To address these issues, we developed a new route to obtain nanosized polycrystalline 3C–SiC by a green and simple method, at temperatures as low as 1200 °C. We start from a cheap, non-toxic material, polycarbosilane (PCS), and NaCl which acts as a template. NaCl is inert and can be easily removed by washing with water.

By carefully tuning the NaCl/PCS weight ratio, different SiC structures were obtained (Fig. 1).

Experimental

Materials

[a]Materials Research Laboratory, University of Nova Gorica, Nova Gorica, SI-5000, Slovenia. E-mail: mirela85.dragomir@gmail.com

[b]Department of Chemistry and Chemical Biology, McMaster University, 1280 Main Street West, Hamilton, Ontario, L8S 4M1, Canada

[c]University of Electronic Sciences and Technology of China, Institute of Fundamental and Frontier Science, North Jianshe Road No. 4 Section 2, Chengdu, 610054, China
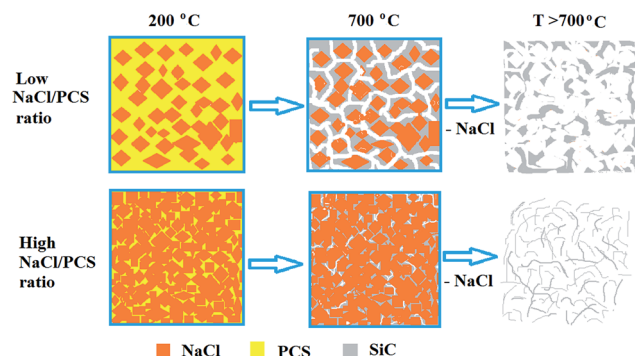
PCS was purchased from Nabond (MW = 1500–2500), while tetrahydrofuran (THF, anhydrous, 99.7%) and NaCl (99+%)

Fig. 1 Schematic representation of the process for the synthesis of 3C–SiC nanoflakes in a NaCl powder template.

were purchased from Alfa Aesar. Ar (99.999%) was used as the inert atmosphere. All the chemicals were used as received, without further purification.

In the typical synthesis procedure, NaCl was first manually ground and then soaked in a 5 wt% solution of PCS in THF to obtain a thick paste. After the THF evaporated, the PCS/NaCl mixture was loaded into an alumina crucible and heated to 700 °C under an Ar flow for 5 h. In a parallel experiment, dry PCS was added to the NaCl powder and manually ground together for 30 minutes before being loaded in the furnace and heated under the same conditions. The resulted samples (consisting of pyrolyzed PCS and NaCl) were washed several times with deionised H_2O to remove the salt. A dark brown powder was recovered through centrifugation and was subsequently air dried at 55 °C, for few hours. The collected powder (pyrolyzed PCS) was then heated to temperatures between 990–1200 °C for different periods of time to promote the crystallisation of SiC. The yield of SiC was approximately 50 wt% with respect to the initial mass of PCS. Upon examination by scanning electron microscopy, no difference in morphology was observed when a PCS/THF solution or only dry PCS was used. Also, no difference in the morphology of the samples that were ground after the addition of PCS/THF solution and of the samples that were not ground after the NaCl was soaked with PCS/THF solution was noticed.

Characterisation

X-ray diffraction (XRD) analysis was performed with a PANalytical X'pert Pro diffractometer with Cu K_α radiation and an X'celerator detector. The diffraction patterns were recorded in the 2-theta range from 20° to 90° with a step size of 0.5° and a collection time of 100 s per step. The diffraction patterns were analyzed for the phase composition using H'Pert HighScore software. For the estimation of the crystallite size using the Scherrer equation, the full width at half maximum (FWHM) of the most intense peak was used.

The microstructure was investigated with a scanning electron microscope (SEM) model JEOL JSM 7100F, in a secondary electron mode. For this analysis, the samples were first dispersed in ethanol, then sonicated in an ultrasonic bath for 15 minutes. Afterwards, a drop of this dispersion was added onto

a Si wafer. After the solvent evaporated, the Si wafer was fixed on the sample holder using a carbon tape. An accelerating voltage of 20 kV was used for all the samples.

Transmission electron microscopy (TEM) analysis was performed with a transmission electron microscope model JEOL JEM 2100 HR, operating at 200 kV. For the TEM analysis, a dilute dispersion of SiC flakes in ethanol was first prepared. The dispersion was transferred to an ultrasonic bath for 15 min and then deposited on a lacey carbon-coated TEM grid by immersing the grid for few seconds in this dispersion and then air dried.

Fourier transform infrared (FT-IR) spectra were recorded in attenuated total reflectance (ATR) mode on a FT-IR spectrophotometer (Perkin Elmer Spectrum 100 FT-IR) equipped with TGS detector and an ATR module. For each measurement, the powder was pressed on the ATR (diamond) window ($d = 2$ mm) and each spectrum was collected from 32 scans accumulation, each with a nominal resolution of 4 cm^{-1} in the region 400–4000 cm^{-1}. The background was measured with the ATR module without any sample.

The room temperature Raman spectra were recorded on the powder, in a 180° backscattering geometry, after 10 recordings, with a Horiba Jobin-Yvon Lab RAM HR spectrometer equipped with a holographic notch filter and a CCD detector, by using the 632.8 nm excitation line of a 20 mW HeNe laser. The samples were placed on an Olympus BX 40 microscope equipped with a 50× objective and the laser beam was focused on the sample to give a spot size of 1 μm. The spectra were recorded in the range of 50–4000 cm^{-1}.

The texture characteristics were determined by low-temperature (77.4 K) nitrogen adsorption in a Quantachrome Instruments NOVA 1200e (USA) apparatus. The nitrogen adsorption–desorption isotherms were analyzed to evaluate the following parameters: the specific surface areas (S_{BET}) determined on the basis of the BET equation, the total pore volume (V_t) estimated in accordance with the Gurvich rule at a relative pressure close to 0.99, and the pore size distribution (PSD) calculated using the BJH method.

Results and discussions

The microstructure of the as-obtained samples was investigated by SEM. It was found that the morphology of the particles changed drastically with the NaCl/PCS weight ratio. Big particles with dimensions ranging from 80–100 μm formed when the NaCl/PCS ratio was 1 : 1 (Fig. 2A). These particles were microcracked but with some smooth surfaces formed at the faces of the NaCl crystallites.

As the NaCl/PCS ratio increased to 5 : 1, the particles size decreased to about 60 μm (Fig. 2B). The morphology changed so that the particles show cavities with non-uniform shapes and volumes reflecting the morphology of the NaCl template. With the increase in the NaCl/PCS ratio to 10 : 1 (Fig. 2C), the mean particle size decreased to about 20 μm. In this case, the particles have a foamy-like structure. The morphology remained the same for the ratio of 20 : 1 (Fig. 2D). It appears that the cell walls become thinner as bigger cavities are formed. At a further
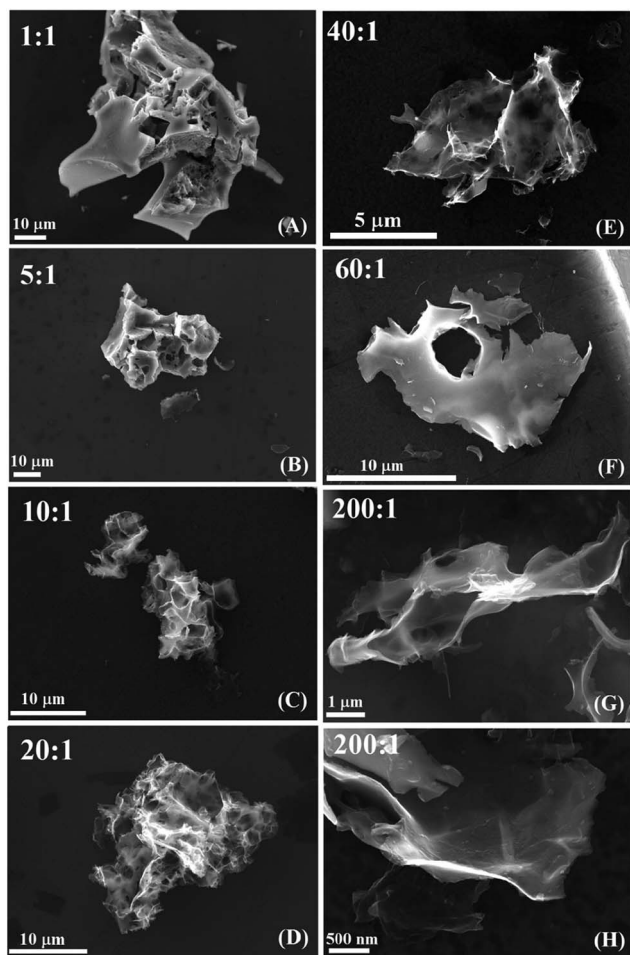
Fig. 2 SEM images of the SiC samples obtained by pyrolysis of PCS at different NaCl/PCS ratios.

increase in the NaCl/PCS ratio to 40 : 1 the particles split to form a "W" shape (Fig. 2E).

For the NaCl/PCS ratio of 60 : 1, the particle size remained in the range of 5 to 10 μm. At this ratio, the particles look like thin flakes with some holes of few micrometers in diameter (Fig. 2F). No noticeable change in the morphology of the particles can be seen for the NaCl/PCS ratio of 200 : 1 (Fig. 2G and H). It is difficult to estimate the thickness of these flakes since they are non-uniform, but from the SEM analysis it can be approximated that they are about 5 nm at the edges and up to 50–60 nm in the thicker regions.

Aforementioned findings indicate the existence of a critical NaCl/PCS ratio of about 40 : 1, at which the sheet-like structure of the SiC particles prevails. We assume that the reason behind this is a critical film thickness of the melted PCS film. Below this thickness, the liquid film ruptures.

To estimate this value, a theoretical critical film thickness of the liquid PCS on the NaCl surfaces, h_c, was calculated using an equation developed by Manev and Nguyen[37] (eqn (1)):

$$h_c = (A\lambda_c^2/128\sigma)^{1/4} \tag{1}$$

where A is the non-retarded Hamaker constant, λ_c is a critical wavelength which can be approximated with $1/r$, (r is the film radius) and σ is the surface tension. Assuming that r of a NaCl particle (with the diameter of a NaCl particle of about 40 μm, as in Fig. 3) is 20 μm, and that the surface tension σ has a value of about 22 dynes cm^{-1} (mJ m^{-2}), for which a Hamaker constant A is about 10–20 J, then from the eqn (1) results that the h_c will have a value of 11 nm. This value represents the thickness of the polymer film before the pyrolysis. Due to the polymer to ceramic conversion, this thickness will further decrease down to few nanometers. Indeed, as SEM analysis revealed, the smallest SiC flake thickness is below 5 nm.

Fig. 4 shows the XRPD patterns of the samples obtained when the pyrolysed PCS (NaCl/PCS ratio of 40 : 1) was heated at different temperatures, in Ar flow. It can be seen that the XRD pattern of the SiC flakes obtained at a temperature of 990 °C shows only a broad peak at 2-theta of 31.7° and this indicates that the flakes obtained at this temperature are amorphous.

At 1000 °C, a long-range order starts to develop as it is suggested by the onset of sharpening of this peak. As expected, a further increase in temperature to 1200 °C leads to a notable difference in the XRD patterns. At this temperature, three peaks that correspond to the characteristic planes of 3C–SiC, (111),
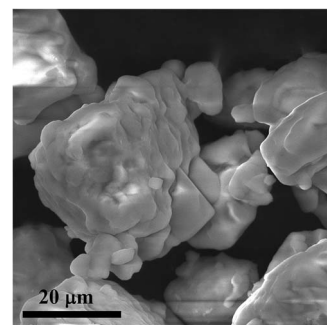

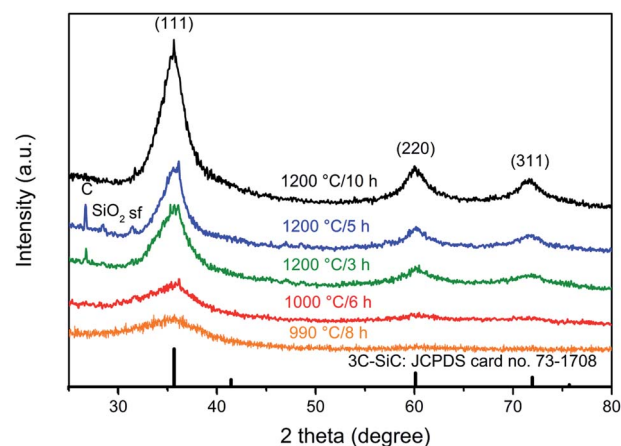**Fig. 3** A SEM image of the NaCl particles used in the synthesis of the SiC nanometer thin flakes.

Fig. 4 XRPD patterns of the solids resulted when the pyrolysed PCS (from a NaCl/PCS ratio of 40 : 1) was heated at different temperatures, in Ar flow.

(220), and (311) are clearly visible. As indicated by the broadness of the SiC diffraction peaks, the thermal treatment at 1200 °C for 3 h results in a SiC with a poor crystallinity and very small crystallite size.

With the increase in the dwell time to 5 h and 10 h, a further increase in the crystallinity and growth of the crystal size occurs as it is suggested by the more intense and sharper diffraction peaks. The mean crystallite size for the sample obtained at 1200 °C/10 h was calculated with Scherrer equation[38] (it was assumed that the peak broadening was caused only by the grain size, the microstrain and inhomogeneity of the sample were neglected) and it was found to be 3.65 nm.

Two additional small peaks corresponding to carbon and SiO_2 phases are also noticeable but only for the samples obtained at 1200 °C after 3 and 5 h, respectively. It is well-known that the conversion of PCS to SiC will always result in the formation of residual carbon and some SiO_2 – usually as a protective silica layer on the SiC material.[39] While the presence of C is due to a nonstoichiometric C/Si ratio in the PCS, SiO_2 can result from absorption of oxygen or moisture in raw PCS or oxygen entering the system during pyrolysis.

Judging only from the XRD analysis, one can see that the sample obtained at 1200 °C/10 h is composed of only 3C–SiC. No impurities are detected for this sample, only one additional small peak located at 2-theta of 31.7°, which corresponds to the staking faults, sf. Sf are the most common defects in 3C–SiC and they are regions of incorrect stacking of the crystal planes or twin boundaries.[40,41] However, evidence for the presence of some turbostratic C in this sample was later found from TEM and Raman analyses.

To further investigate the microstructure and phase composition of the SiC flakes, TEM, Raman, and IR analyses were performed. TEM images on the SiC samples obtained at different temperatures are shown in Fig. 5–8.

Fig. 5A–D shows a selection of TEM and HRTEM (as insets) images of samples obtained at different temperatures and dwell times. At a temperature of 1000 °C/6 h (Fig. 5A) the samples look

Fig. 6 TEM images of a SiC flake obtained at 1200 °C/5 h, from a NaCl/PCS ratio of 40 : 1.

Fig. 7 TEM images of a SiC flake obtained at 1200 °C/10 h, from a NaCl/PCS ratio of 40 : 1. The inset is the corresponding fast Fourier transform pattern.
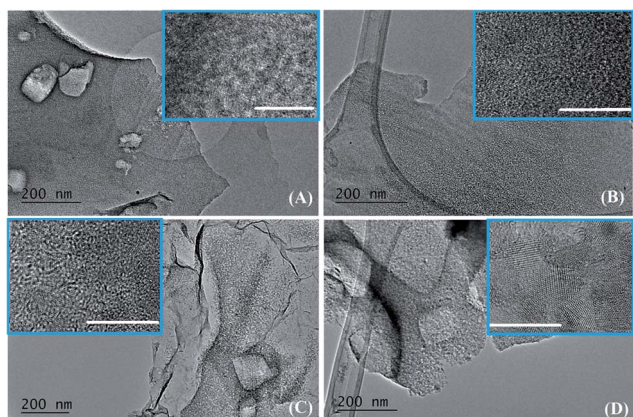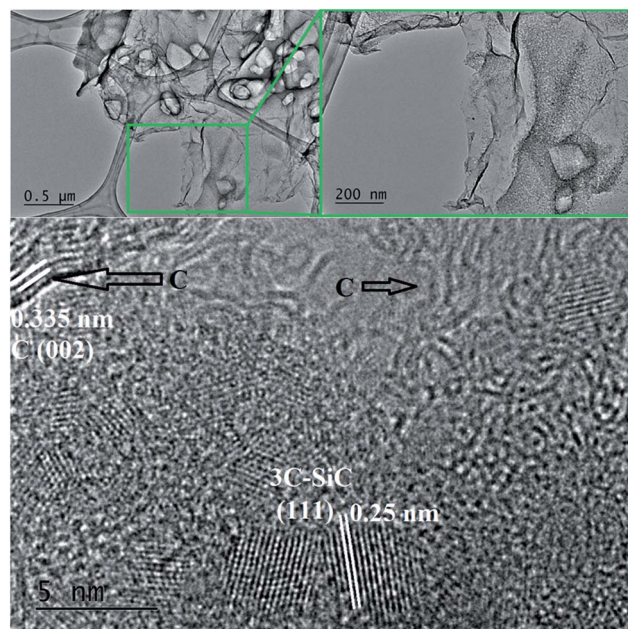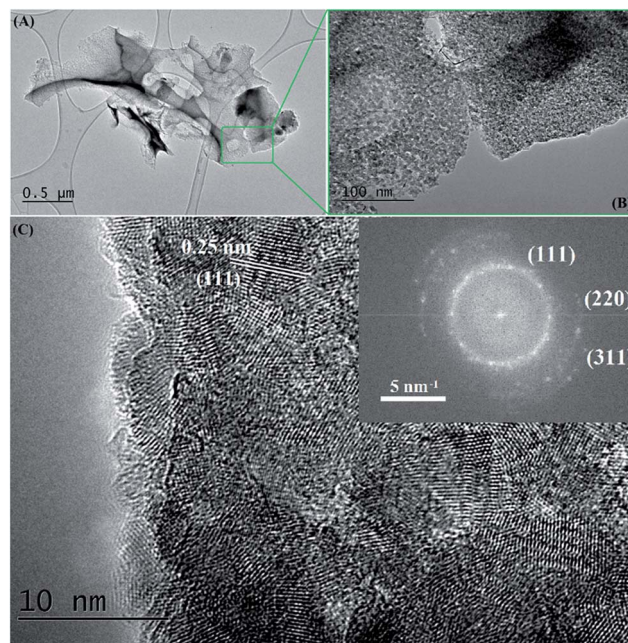

Fig. 5 TEM images of the SiC flakes obtained from a NaCl/PCS ratio of 40 : 1, heated at different temperatures and for different periods of time: 1000 °C/6 h (A), 1200 °C/3 h (B), 1200 °C/5 h (C), and 1200 °C/10 h (D). The insets are a high magnification image on the corresponding flake. The scale bar in all the insets is 10 nm.

like thin sheets with some rectangular holes (produced after the deionised water washed away the NaCl particles) and there is no obvious long-range order (see the inset in Fig. 5A).

A higher temperature of 1200 °C with a dwell time of 3 h does not result in a significant change of the texture or crystallinity. In the inset in Fig. 5B there is though a suggestion of some embryonic ordering from the presence of few SiC crystalline
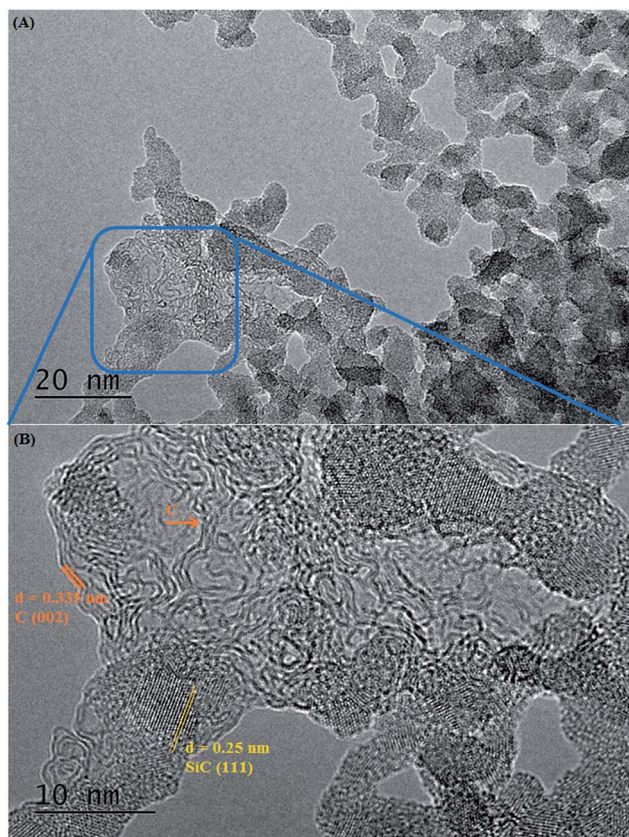
Fig. 8 (A) Additional TEM image of a SiC flake obtained at 1200 °C/10 h from a NaCl/PCS ratio of 40 : 1; (B) this HRTEM image shows that an additional phase with the interplanar distance of 0.335 nm (carbon) is sometimes observed among the SiC nanocrystals.

areas in an amorphous matrix. A further small increase in the dwell time from 3 to 5 h leads to a drastic change in both texture and crystallinity. Fig. 5C clearly shows the presence of small crystallites in a thin sheet-like matrix. A closer look at the inset in Fig. 5C reveals that those spots are circular crystalline structures of about 2 nm in diameter with clearly visible lattice fringes. After 10 h at 1200 °C, these crystallites grew to a size of about 4 nm and became interconnected as a result of the complete crystallisation and crystal growth (Fig. 5D). TEM analysis is in agreement with the XRD data which showed that the crystallinity of the samples increases progressively with increasing the dwell time from 3 to 10 h at 1200 °C. Additional TEM images on the SiC flakes thermally treated at 1200 °C/5 h are shown in Fig. 6. These images of SiC flakes freely suspended on a lacey carbon coated TEM grid further confirm their sheet-like morphology. The SiC samples also have few voids which were probably produced after the deionised water washed away the NaCl particles. Nanocrystallites of 3C–SiC ($d = 0.25$ nm) with an average size of 2.7 nm (determined with the ImageJ software) and different forms of carbon (turbostratic and onion-like carbon, with $d = 0.335$ nm) can also be observed in these images.

Bright field TEM images of the sample obtained at the same temperature of 1200 °C but with a 10 h dwell time are shown in

Fig. 7. At a closer look (Fig. 7B), it can be seen that the flake is polycrystalline and it is composed only of SiC crystallites with average size 3.7 nm (most of them being between 2–5 nm), value which is in excellent agreement with the crystallite mean size calculated by XRD (3.65 nm). Crystallites are randomly oriented and different orientations are observed in the TEM image, distinguishable from different interplanar distances (0.25 nm for the (111) plane but also along the (220) and (311) planes) as shown in the corresponding Fast Fourier Transform (FFT) pattern (in the inset of the Fig. 7C). Additional TEM analyses on a different part of this flake (Fig. 8) show that some of the flakes are composed not only of 3C–SiC nanocrystallites ($d = 0.25$ nm), but also graphene-like or onion-like carbon (with $d = 0.335$ nm).

Raman analysis (Fig. 9) also suggests that some free carbon is present in this sample. In Fig. 9, the two Raman spectra (for the sample obtained at 1000 °C/6 h and after crystallisation – 1200 °C/10 h) look very similar. The amorphous sample (1000 °C/6 h) shows two main peaks at 1322 and 1603 cm^{-1}, plus some small peaks at around 458, 611, 864, 959, 1160, 2623 and 2911 cm^{-1}. The band located at 1160 cm^{-1} corresponds to the ν_1 mode of transpolyacetylene;[42,43] at 1322 cm^{-1} is the D band of carbon (so called "disorder" band) which corresponds to the zone center phonons of E_{2g} symmetry and it is associated with the structural imperfections or symmetry loss. The peak at 1603 cm^{-1} is the G (or graphitic) mode which is assigned to the A_{1g} mode (in plane vibrational mode) of carbon. The peak at 2623 cm^{-1} is a second order overtone of the D mode (also named "2D") whereas the peak at 2911 cm^{-1} is the D' or D + G peak (a combination scattering peak). An increase in the temperature to 1200 °C resulted in disappearance of the peak at 1160 cm^{-1}, a redshift of the G peak from 1603 to 1589 cm^{-1}, and a narrowing of both D and G peaks. The redshift and narrowing of the G peak might indicate an increase in the ordering of the carbon phase.[44] The I_D/I_G ratio (I is the intensity of the peak) is related to the degree of carbon amorphisation.[45] In our case, the I_D/I_G ratio is having a value of 1.43 and 1.37, for the amorphous and crystalline SiC,
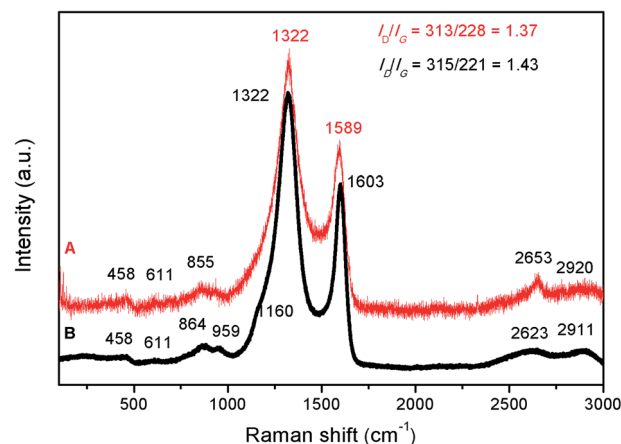

Fig. 9 Raman spectra of SiC samples obtained at two different temperatures, before (1000 °C/6 h – spectrum B) and after crystallisation (1200 °C/10 h – spectrum A).
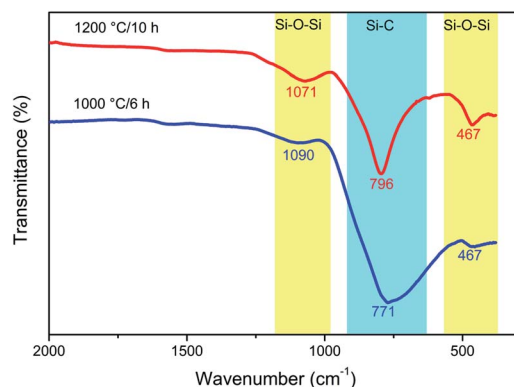
Fig. 10 ATR spectra of two SiC samples obtained at two different temperatures, before (1000 °C/6 h) and after (1200 °C/10 h) crystallisation.

Table 1 Specific surface area, S_{BET}, total pore volume, V_t, and pore dimensions, D, of the samples obtained at 700 °C/5 h (before crystallisation) and at 1200 °C/10 h (after crystallisation) from different NaCl/PCS ratios

NaCl to PCS weight ratio	Obtained at 700 °C			Obtained at 1200 °C		
	S_{BET} ($m^2 g^{-1}$)	V_t, ($cm^3 g^{-1}$)	D (nm)	S_{BET} ($m^2 g^{-1}$)	V_t, ($cm^3 g^{-1}$)	D (nm)
1 : 1	8	0.02	7	4	0.05	4.5
5 : 1	13	0.02	5	9	0.01	5.8
10 : 1	8	0.02	9.5	24	0.03	4.6
20 : 1	10	0.02	10	64	0.10	6
40 : 1	15	0.07	19	169	0.19	4.5
60 : 1	21	0.09	16	68	0.12	7.2
200 : 1	163	0.75	1.81	72	0.26	14

respectively and this further suggests that in both samples, the carbon could exist in the form of few graphene layers.

The small peaks located at 458 and 611 cm^{-1} correspond to the Si–O–Si bonds, whereas the ones located at about 860 and 959 cm^{-1} are probably the TO and LO Raman modes of SiC. Due to a better Raman scattering efficiency of the C–C bonds compared to the Si–C ones, and for such small SiC crystallites, the Raman lines characteristic of crystalline SiC become almost unobservable.[46] The residual carbon observed along with the SiC phase can be beneficial in photocatalytic processes where it can serve as electron-accepting sites, facilitating the interface charge separation. But if desired, this residual carbon can also be removed by heating in air at approximately 600 °C.

ATR analysis of the samples obtained at 1000 °C/6 h and 1200 °C/10 h (Fig. 10) shows that both samples consist of mainly SiC. At 1000 °C, a broad absorption band at 771 cm^{-1} and two small shoulders at 467 and 1090 cm^{-1} are observed. The strongest band (771 cm^{-1}) corresponds to the Si–C bond stretching mode, while the weak absorption bands (467 and 1090 cm^{-1}) could be assigned to Si–O symmetric and asymmetric stretching modes. With an increase in temperature to 1200 °C and, therefore, an increase in the crystallinity, these bands become narrower. As also indicated by ATR analysis, the SiC obtained at 1200 °C/10 h contains a very small amount of silicon dioxide. This SiO$_2$ can be removed by washing with a small amount of diluted hydrofluoric acid.[47]

To obtain quantitative morphologic information about the samples, nitrogen adsorption was measured at 77.4 K. The specific surface area was calculated using the BET method (S_{BET}). The isotherms were analysed to determine the total pore volume (V_t) and the pore size distribution (PSD).

To investigate the effect of the NaCl/PCS ratio on the S_{BET}, fourteen samples were selected, as shown in Table 1.

As already revealed by SEM, the BET analyses indicate that a fine tuning of the NaCl/PCS ratio clearly results in the evolution of diverse morphologies. For the samples obtained at the temperatures lower than the crystallisation temperature, the S_{BET} increased with the NaCl/PCS ratio from a value of 8 m^2 g^{-1} (1 : 1 ratio) up to a maximum value of 163 m^2 g^{-1} (200 : 1 ratio).

This high S_{BET} is associated with a very high value of the V_t of 0.75 cm^3 g^{-1}. Also the S_{BET} of the crystalline samples increased with the NaCl/PCS ratio, from 4 m^2 g^{-1} (1 : 1) up to a value of 72 m^2 g^{-1} (200 : 1). When NaCl/PCS ratio was below 10 : 1, the S_{BET} of the SiC obtained at 1200 °C was lower than that at 700 °C. At 1200 °C, as the crystallisation occurs, Si–C bonds rearrange to form a more dense structure which could lead to a decrease of the S_{BET}. The samples obtained from a NaCl/PCS ratio ≥ 20 : 1 showed a bigger S_{BET} at 1200 °C than at 700 °C, except for the sample obtained from a NaCl/PCS ratio of 200 : 1, which shows decreased S_{BET}. It is interesting to observe that at 1200 °C, the largest S_{BET} belongs to the sample obtained from a NaCl/PCS ratio of 40 : 1.

Conclusions

In this work, a facile synthetic route to 3C–SiC nanoflakes by pyrolysis of PCS in a NaCl template at 700 °C, followed by crystallisation at 1200 °C, was developed. It was found that the weight ratio between NaCl and PCS is dictating the morphology of the SiC particles. A critical NaCl/PCS ratio for the formation of the nanoflakes has been determined to be around 40 : 1. These nanometer thin SiC flakes exhibit a high specific surface area of up to 169 m^2 g^{-1} and a high total pore volume of up to 0.75 cm^3 g^{-1} – properties which can be finely tuned by the adjustment of the NaCl/PCS ratio.

This method is a simple, versatile and robust way for the production of SiC nanostructures. Such a facile synthetic method could bring nanostructured SiC one step closer to the ultimate goal of practical applications such as in Li-ion batteries, for hydrogen evolution and/or storage, as anticorrosive surfaces, solar cells, fuel cells and other applications.

Acknowledgements

Notes and references

1 D. H. Van Dorp, N. Hijnen, M. Di Vece and J. J. Kelly, *Angew. Chem., Int. Ed.*, 2009, **48**, 6085.

2 J. Fan and P. K. Chu, *Small*, 2010, **19**, 2080.

3 E. S. Saddow, *Silicon Carbide Biotechnology: A Biocompatible Semiconductor for Advanced Biomedical Devices and Applications*, Elsevier, Amsterdam, 2012.

4 W. H. Backes, P. A. Bobbert and W. van Haeringen, *Phys. Rev. B: Condens. Matter Mater. Phys.*, 1994, **49**, 7564.

5 J. Fan and P. K. Chu, *Silicon Carbide Nanostructures: Fabrication, Structure, and Properties*, Springer International Publishing, Switzerland, 2014.

6 J. Y. Fan, X. L. Wu and P. K. Chu, *Prog. Mater. Sci.*, 2006, **51**, 983.

7 J. Fan, H. Li, J. Jiang, L. K. Y. So, Y. W. Lam and P. K. Chu, *Small*, 2008, **4**, 1058.

8 Y. Zakharko, T. Nychyporuk, L. Bonacina, M. Lemiti and V. Lysenko, *Nanotechnology*, 2013, **24**, 055703.

9 X. Lin, S. Lin, Y. Xu, A. Hakro, T. Hasan, B. Zhang, B. Yu, J. Luo, E. Li and H. Chen, *J. Mater. Chem. C*, 2013, **1**, 2131.

10 W. Zhou, L. Yan, Y. Wang and Y. Zhang, *Appl. Phys. Lett.*, 2006, **89**, 013105.

11 J.-Y. Hao, Y.-Y. Wang, X. L. Tong, G. Q. Jin and X.-Y. Guo, *Int. J. Hydrogen Energy*, 2012, **37**, 15038.

12 Z. Cheng, F. Bing, Q. Liu, Z. Zhang and X. Fang, *J. Mater. Chem. A*, 2015, **3**, 4652.

13 S. D. T. Kumari, D. Jeyakumar and T. P. Kumar, *RSC Adv.*, 2013, **3**, 15028.

14 C. He, X. Wu, J. Shen and P. K. Chu, *Nano Lett.*, 2012, **12**, 1545.

15 G. Mpourmpakkis and G. E. Froudakis, *Nano Lett.*, 2006, **8**, 1581.

16 M. Wang, J. Chen, X. Liao, Z. Liu, J. Zhang, L. Gao and Y. Li, *Int. J. Hydrogen Energy*, 2014, **39**, 14581.

17 G. Mishra, K. M. Parida and S. K. Singh, *ACS Sustainable Chem. Eng.*, 2015, **3**, 245.

18 K. V. Emtsev, A. Bostwick, K. Horn, J. Jobst, G. L. Kellogg, L. Ley, J. L. McChesney, T. Ohta, S. A. Reshanov, J. Röhrl, E. Rotenberg, A. K. Schmid, D. Waldmann, H. B. Weber and T. Seyller, *Nat. Mater.*, 2009, **8**, 203.

19 P. Mavinakuli, S. Wei, Q. Wang, A. B. Karki, S. Dhage, Z. Wang, D. P. Young and Z. Guo, *J. Phys. Chem. C*, 2010, **114**, 3874.

20 Z. Guo, T. Y. Kim, K. Lei, T. Pereira, J. G. Sugar and H. T. Hahn, *Compos. Sci. Technol.*, 2008, **68**, 164.

21 J. Chen, J. Zhang, M. Wang and Y. Li, *Sens. Actuators, B*, 2014, **201**, 402.

22 J. Chen, X. Liao, M. Wang, Z. Liu, J. Zhang, L. Ding, L. Gao and Y. Li, *Nanoscale*, 2015, **7**, 6374.

23 S. Yang, W. Cai, H. Zeng and X. Xu, *J. Mater. Chem.*, 2009, **19**, 7119.

24 T. Seeger, P. Kohler-Redlich and M. Rühle, *Adv. Mater.*, 2000, **12**, 279.

25 Y. Y. Choi and D. J. Choi, *CrystEngComm*, 2013, **15**, 6963.

26 G. W. Meng, Z. Cui, L. D. Zhang and F. Philipp, *J. Cryst. Growth*, 2000, **209**, 801.

27 S. Chabi, H. Chang, Y. Xia and Y. Zhu, *Nanotechnology*, 2016, **27**, 075602.

28 J. Chen, Q. Shi, L. Gao and H. Zhu, *Phys. Status Solidi A*, 2010, **207**, 2483.

29 J. Chen, J. Zhang, M. Wang, L. Gao and Y. Li, *J. Alloys Compd.*, 2014, **65**, 168.

30 L. Xin, Q. Shi, J. Chen, W. Tang, N. Wang, Y. Liu and Y. Lin, *Mater. Charact.*, 2012, **65**, 55.

31 R. D'Amato, M. Falconieri, S. Gagliardi, E. Popovici, E. Serra, G. Terranova and E. Borsella, *J. Anal. Appl. Pyrolysis*, 2013, **114**, 461.

32 X. Liu, M. Antonietti and C. Giordano, *Chem. Mater.*, 2013, **25**, 2021.

33 J. Zhu, Z. Liu, X. L. Wu, L. L. Xu, W. C. Zhang and P. K. Chu, *Nanotechnology*, 2007, **18**, 365603.

34 I. K. Sung, S. B. Yoon, J.-S. Yu and D.-P. Kim, *Chem. Commun.*, 2002, **14**, 1480.

35 K.-H. Park, I.-K. Sung and D.-P. Kim, *J. Mater. Chem.*, 2004, **14**, 3436.

36 N. Baccile, F. Babonneau, B. Thomas and T. Coradin, *J. Mater. Chem.*, 2009, **19**, 8537.

37 E. D. Manev and A. V. Nguyen, *Adv. Colloid Interface Sci.*, 2005, **114–115**, 133.

38 P. Scherrer, *Nachr. Ges. Wiss. Goettingen, Math.-Phys. Kl.*, 1918, **1918**, 98.

39 E. Bouillon, F. Langlais, E. Pailler, E. Naslain, F. Cruege, J. C. Houng Sarthou, A. Delpuech, C. Laffon, P. Lagarde, M. Monthioux and A. Oberlin, *J. Mater. Sci.*, 1991, **26**, 1333.

40 E. J. Olivier and J. H. Neethling, *Int. J. Refract. Met. Hard Mater.*, 2009, **27**, 443.

41 U. Lindefelt, H. Iwata, S. Öberg and P. Briddon, *Phys. Rev. B: Condens. Matter Mater. Phys.*, 2003, **67**, 155204.

42 A. C. Ferrari and J. Robertson, *Philos. Trans. R. Soc., A*, 2004, **362**, 2477.

43 C. Castiglioni, M. Tommasini and G. Zerbi, *Philos. Trans. R. Soc., A*, 2004, **362**, 2425.

44 S. Karlin and P. Colomban, *J. Raman Spectrosc.*, 1997, **28**, 219.

45 A. C. Ferrari and J. Robertson, *Phys. Rev. B: Condens. Matter Mater. Phys.*, 2001, **64**, 075414.

46 E. Bouillon, F. Langlais, R. Pailler, R. Naslain, F. Cruege and P. V. Huong, *J. Mater. Sci.*, 1991, **26**, 1333.

47 G. Wei, W. Qin, K. Zheng, D. Zhang, J. Sun, J. Lin, R. Kim, G. Wang, P. Zu and L. Wang, *Cryst. Growth Des.*, 2009, **9**, 1431.